AQUA
Water Infrastructure, Ecosystems and Society

IWA PUBLISHING

 AQUA — Water Infrastructure, Ecosystems and Society Vol 73 No 9, 1789 doi: 10.2166/aqua.2024.322

Optimization of the direct synthesis of hydroxyapatite from aquaculture wastewater using Response Surface Methodology

Siti Solihah Rasdei[a], Norhafiza Ilyana Yatim[b], Nora'aini Ali[a,*] and Nor Azman Kasan[b]

[a] Faculty of Ocean Engineering Technology, Universiti Malaysia Terengganu, 21030 Kuala Nerus, Terengganu, Malaysia
[b] Higher Education Center of Excellence (HICoE), Institute of Tropical Aquaculture and Fisheries, Universiti Malaysia Terengganu, Mengabang Telipot, Kuala Terengganu, Terengganu, Malaysia
*Corresponding author. E-mail: noraaini@umt.edu.my

ABSTRACT

The utilization of phosphorus-rich aquaculture wastewater (AQW) offers a promising avenue for the recovery of valuable compounds, particularly hydroxyapatite (HAp) materials. The aim of this study was to use Response Surface Methodology (RSM) to explore the potential of recycling AQW directly to produce HAp compounds due to its considerable commercial value. Using the Central Composite Design (CCD) within the RSM, about three parameters, such as pH (between 9 and 11), contact time (between 36 and 60 h), and stirring rate (between 120 and 240 rpm) were optimized. The response of the CCD, crystallinity, was evaluated by X-ray diffraction analysis. The optimized conditions, pH of 10, contact time of 48 h, and stirring rate of 180 rpm resulted in HAp crystals characterized according to the Joint Committee on Powder Diffraction Standard, JCPDS (9,003,549), with a crystallite size of 23.6 nm. Remarkably, about 89.97% of the phosphate was removed from the AQW under these conditions, emphasizing the potential of this approach to reduce waste while producing a commercially viable product. The study highlights the viability of developing a zero-waste industry, and the utilization of calcium apatite-based products derived from AQW offers a promising socio-economic strategy for the future.

Key words: aquaculture wastewater, calcium apatite-based, central composite design, hydroxyapatite, optimization, Response Surface Methodology

HIGHLIGHTS

- Aquaculture wastewater acts as a resource for the recovery of valuable compounds.
- Potential calcium apatite-based compounds were produced under different conditions.
- Modeling from RSM was acheived to optimize the possibility of parameter efficiency to achieve the objective.
- Optimum conditions for the highest recovery of phosphorus from aquaculture wastewater were studied.
- The zero-waste approach in industry has long-term benefits in the future.

GRAPHICAL ABSTRACT

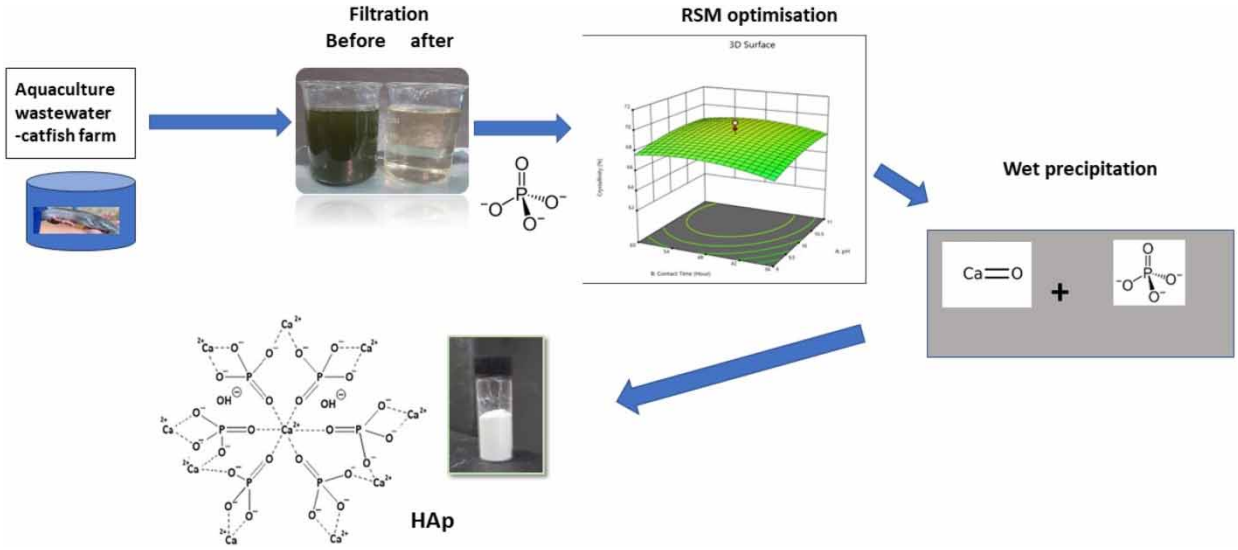

1. INTRODUCTION

Aquaculture plays a significant role in the economies of countries, contributing significantly to gross domestic product (GDP) through local seafood supply and exporting valuable commodities (Kurniawan *et al.* 2021). By 2020, the cumulative aquaculture production reached 400,017 metric tons (mt), with a wholesale value of RM3,114,731. A freshwater aquaculture system is a technique for cultivating freshwater aquaculture in various environments such as fishponds, fish pens, reservoirs, former mining ponds, rice fields, or canvas tanks. Species such as tilapia, catfish, and carp are usually farmed in freshwater lakes, ponds, rivers, or reservoirs for commercial purposes (Mat Zain & Lee 2022). However, in the pre-harvest phase, wastewater produced is often contaminated with particles and nutrients from sources such as fertilizers, spilt feed, and reared animal waste (Nizam *et al.* 2020).

Phosphorus (P) is one of the most important elements and nutrients required for the growth of aquatic plants and also as food for other microorganisms living freely in water bodies and rivers (Anawar & Chowdhury 2020; Tiwari & Pal 2022). However, excessive phosphorus levels in water bodies can trigger excessive algae growth, indicating eutrophication. A low P concentration of 0.02 mg/L is sufficient to trigger eutrophication and disrupt aquatic life by reducing dissolved oxygen content and hindering sunlight, eventually leading to depopulation and development of underwater dead zones (Jin *et al.* 2019; Yang *et al.* 2022; Dadi *et al.* 2023). Although nitrogen is also a contributing element to eutrophication, the role of phosphorus plays a major role (Schindler *et al.* 2016).

The recovery of P is a major challenge. Since the demand for P in the industry itself is not too impressive, most of the P is preferably recovered as fertilizer and other valuable compounds. In particular, the recovery of phosphate from agricultural wastewater in the form of hydroxyapatite (HAp) by chemical precipitation is of utmost practical importance for completing the P cycle (Cichy *et al.* 2019). Former studies suggested that P recovery involves self-crystallization between calcium and phosphorus, toward the amorphous calcium phosphate precursor and subsequent growth of HAp. The pH will change during the calcium–phosphate crystallization interaction, indicating the involvement of proton release mechanism (Li *et al.* 2022). HAp [$Ca_{10}(PO_4)_6OH_2$] is a bioceramic material which has been used over the decades. It has durable thermal and chemical properties which have been used widely in medicine, wastewater treatment, and various industries (Akpan *et al.* 2021). HAp is synthesized by different methods depending on the structure and apparent properties (Sadat-Shojai *et al.* 2013). The simplest and cheapest method is the wet precipitation method. The wet precipitation method allows the size and morphology of nanoparticles to be regulated, leading to the formation of nanoparticles under certain conditions (Sajid & Płotka-Wasylka 2020; Shrestha *et al.* 2020).

In modern research practice, the integration of computer-aided methods has become a cornerstone for the further development of scientific investigations (Deng *et al.* 2023, 2024; Li *et al.* 2024). Through the use of computational modeling and

analysis, researchers can explore complicated systems, fine-tune experimental parameters, and gain insights beyond the scope of conventional experimental methods (Singh 2021, 2023; Singh & Samsher 2021, 2022). The present study utilized RSM, a computational tool, to investigate the recovery of HAp from aquaculture wastewater (AQW) under specific parameter conditions. The materials obtained by RSM optimization were then analyzed and compared with commercial HAp to evaluate the physicochemical properties. This holistic approach not only increases the efficiency and precision of the present study but also creates a robust framework for addressing the challenges associated with sustainable resource management and waste reduction.

The development of aquaculture industries on a commercial scale shows that considerable amounts of phosphorus and nitrogen waste are produced. The abundance of these nutrients represents a promising opportunity for wastewater treatment aimed at zero waste, environmental friendliness and economic benefits. Proper management of this wastewater by converting pollutants into useful compounds for various applications supports a circular economy that reduces environmental impact while creating economic value and is a reliable new pathway to environmentally conscious and economically viable solutions. Thus, exploring the potential of using phosphorus-rich AQW for the recovery of valuable compounds, particularly HAp materials, opens up new avenues for resource recovery. Consequently, by understanding the potential impact of aquaculture on the aquatic environment and understanding the measures can be considered to minimize the environmental impact and it would be beneficial for the long-term sustainability of the sector. Phosphorus recovery and reuse are highly desirable. Therefore, this study focuses on the recovery of the element phosphorus from AQW to produce HAp, a valuable material. This approach can, therefore, reduce phosphorus pollution and increase the production of mineral phosphate in useful material.

2. METHODS

2.1. Materials and sample collection

Chemicals used in this experiment included calcium oxide (CaO) purchased from Sigma Aldrich, and diammonium hydrogen phosphate [$(NH_4)_2HPO_4$] and sodium hydroxide (NaOH) from Supelco. The freshwater AQW sample containing phosphate (P) was obtained from catfish farms at the Hatchery Centre, Universiti Malaysia Terengganu. For preservation of the P content, the wastewater sample was freshly collected and filtered to remove moss and algae, and then stored in the freezer for at least 2 days prior to use. The concentration of phosphate (P) in wastewater before and after the recovery was measured by Ion Chromatography and Anion instrumentation analysis. The final concentration of AQW was examined after the production of HAp to calculate the amount of P taken after the experiment. Figure 1 illustrates the framework of the experimental design used in this study.

2.2. Experimental design

This study applied the RSM with Central Composite Design (CCD) to examine the effects of pH, contact time (hour), and stirring rate (rpm) as parameters to determine the optimum condition for the production of HAp. The reach parameter was analyzed at five specific levels ($-\alpha$, -1, 0, $+1$, $+\alpha$). The number of experiments generated for CCD was defined by Equation (1):

$$Y = 2^x + 2x + C_x \tag{1}$$

where Y is the number of experiments, x is the number of variables, and C_x is the number of center points repetitions. The parameters included a specific range of five levels ($-\alpha$, -1, 0, $+1$, $+\alpha$). There were three variables, six center points, and one repetition in this study. The relationship of independent and response variables is presented in the following second-degree polynomial Equation (2):

$$y = b_0 + \sum_{i=1}^{n} b_i x_i \ + \sum_{i=1}^{n} b_{ii} x_i^2 \ + \sum_{i=1}^{n} \sum_{j>1}^{n} b_{ij} x_{\ i} x_j \tag{2}$$

where b_0 is a constant, b_i are linear coefficients, and x_i is the effect of each variable. The effect of the parameter is $x_i x_j$. b_{ij} is the interaction coefficient and b_{ij} is the coefficient demonstrating the effect of variables $x_i x_i$. Analysis of variance (ANOVA) was used to determine the adequacy of the constructed model to represent the observed data (Ebrahimi *et al.* 2014). The

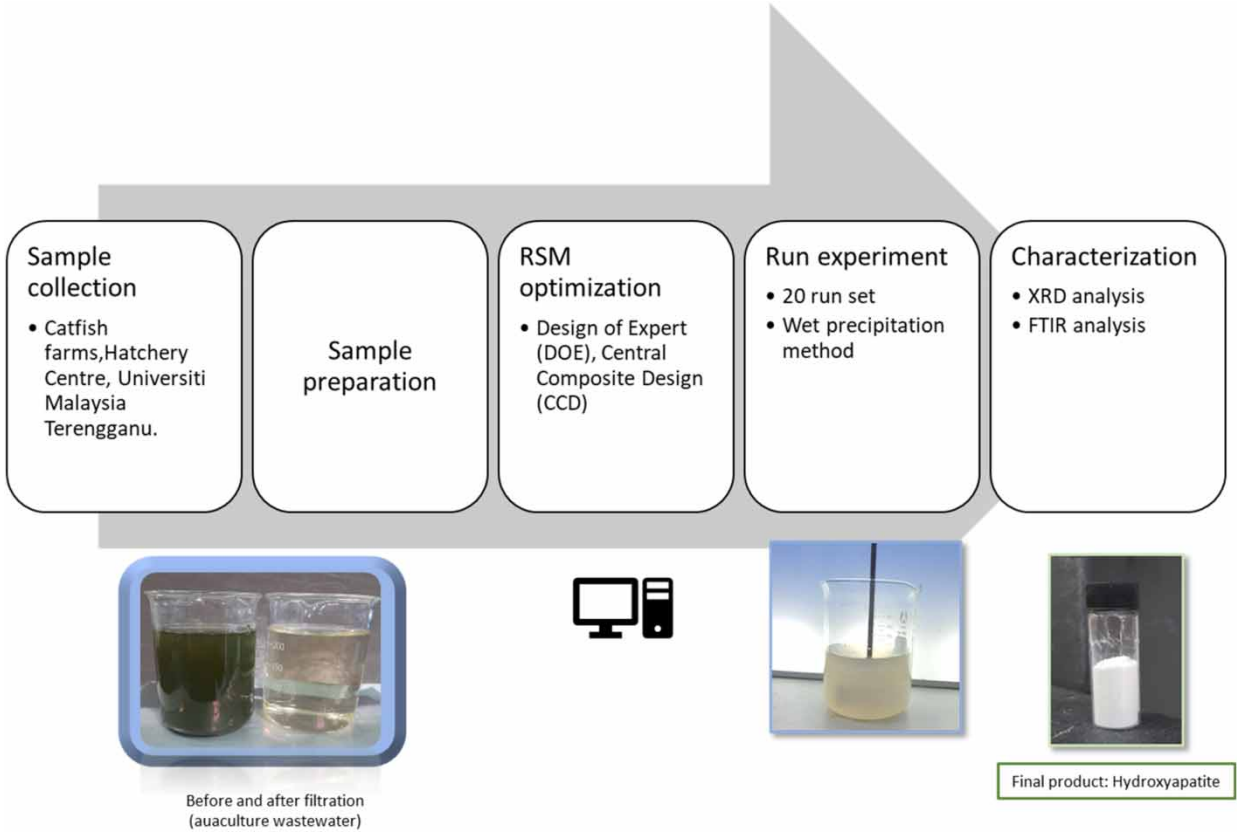

Figure 1 | The experimental framework used in this study.

percentage of variability of the optimization parameters justified by the model is denoted by using the R^2 statistic. The three-dimensional surface plots were portrayed to demonstrate the major and interactive effects of the independent and dependent variables. Table 1 displays the experimental parameters for RSM analysis. This analysis used DOE software (Design Expert13) and CCD.

The CCD generated a total of 20 runs. The wet precipitate method was used to synthesize HAp and the AQW was the source of phosphate and at the same time can be a good medium for phosphate recovery. The pH, contact time, and stirring rate have ranges of 9–11, 36–60, and 120–240, respectively. In total, there were 20 conditions generated based on the CCD and the range of the parameter itself.

2.3. Analysis of physicochemical properties of calcium apatite-based compounds

The samples were characterized using a Rigaku MiniFlex Benchtop X-Ray Diffractometer (XRD) with Cu Kα radiation (λ¼1.5406 Å). It was carried out for 20 sets of samples that were generated by RSM to determine the crystallinity and recorded over the range $2\theta = 10$–80° by step counting at 0.03° with an interval of 0.6 s per data point. The samples were arranged in clumps at the center of a glass sample container and were examined at a high-tension generator set at 30 kV, 15 mA. To examine the crystallinity of materials, the XRD spectrum was analyzed using the computer program PDXL

Table 1 | Parameter with the ranges and values for each

	Parameter	−α	−1	0	+1	+α
A	pH	8	9	10	11	12
B	Contact time	28	36	48	60	68
C	Stirring rate	80	120	180	240	280

software. It was able to identify the crystallinity which can be measured via crystalline to the total area, including the amorphous phase. Measurement of the ratio between the total area covering both amorphous and crystalline phases enables the identification of their respective proportions. The crystalline area is determined by adding up the integrated intensities scattered over a suitable angular interval by the crystalline phase.

The Fourier Transform Infrared (FTIR) spectroscopy (Shimadzu IRTracer-100 model, Japan) was used to analyze the functional group of the sample product. The sample was powdered before analysis. The functional group of compounds was recorded in the region of 650–4,000 cm^{-1} of wavelength and resolution of 2 cm^{-1} as most of the molecules' functional group side chains and crosslink absorb light in this infrared range of the electromagnetic spectrum.

3. RESULTS AND DISCUSSION

3.1. Evaluation of RSM analysis

The determination of crystallinity of HAp under different conditions involving 20 runs include six central points with different combinations of parameters as presented in Table 2. The predicted values were obtained by a model fitting technique via software Design Expert ver. 13 and significantly correlated with the observed (actual) values. Table 2 presents the CCD analysis and Run 2 is considered as the most optimum condition.

The reliability of a model can be evaluated using ANOVA which considers uncertainties in the structural reliability of a model. The theoretical framework for calculating the probability of failure is known as the reliability index of structural systems (Chelladurai *et al.* 2020). Hence, the significance of the quadratic polynomial model was validated by performing the ANOVA test result as shown in Table 3.

The *p*-value represents the degree of significance of each factor. Factors that have a *p*-value (Prob. > *F*) of less than 0.0500 ($p < 0.05$) imply that the model terms are significant with a confidence level of 0.95. The *F*-value of the 'model' obtained in

Table 2 | The predicted values generated using RSM and the actual crystallinity values calculated by the obtained Haps

Run	A pH	B Contact time (h)	C Stirring rate (rpm)	Crystallinity (%)		Compound identification	Joint Committee on Powder Diffraction Standard (JCPDS) No.
				Actual	Predicted		
1	9	60	240	69.14	69.44	Carbonate hydroxyapatite	9,003,553
2	10	48	180	69.40	68.83	Hydroxyapatite	9,011,093
3	10	48	180	68.58	68.83	Hydroxyapatite	9,002,216
4	9	36	120	63.17	63.52	Carbonate hydroxyapatite	9,003,552
5	11	36	120	65.31	65.19	Hydroxyapatite	9,002,215
6	9	36	240	69.06	69.21	Carbonate hydroxyapatite	9,003,551
7	8	48	180	66.42	66.07	Hydroxylellestadite	9,009,375
8	10	28	180	66.73	66.52	Chlorapatite	9,001,263
9	9	60	120	64.79	64.86	Carbonate hydroxyapatite	9,003,555
10	11	60	120	66.07	66.10	Hydroxyapatite-Dental	9,002,218
11	11	60	240	70.02	69.85	Hydroxyapatite-Dental	9,002,224
12	10	48	180	68.64	68.83	Hydroxyapatite	9,003,548
13	10	48	280	71.63	71.48	Carbonate Hydroxyapatite	9,003,555
14	10	48	180	68.53	68.83	Hydroxylellestadite	9,009,375
15	10	68	180	67.52	67.47	Hydroxyapatite-Dental	9,002,226
16	12	48	180	67.98	68.15	Apatite (CaOH)	9,010,050
17	11	36	240	69.93	70.04	Hydroxyapatite-Dental	9,002,223
18	10	48	80	63.71	63.61	Carbonate Hydroxyapatite	9,003,550
19	10	48	180	70.01	68.83	Hydroxyapatite	9,002,214
20	10	48	180	67.85	68.83	Hydroxyapatite	9,003,549

Table 3 | Summary analysis using ANOVA

Source	Sum of squares	df	Mean square	*F*-value	*p*-value	*F-crit*
Model	92.88	9	10.32	30.40	<0.0001	Significant
A, pH	4.30	1	4.30	12.65	0.0052	
B, contact time	1.10	1	1.10	3.25	0.1016	
C, stirring rate	75.59	1	75.59	222.69	<0.0001	
AB	0.0903	1	0.0903	0.2661	0.6172	
AC	0.3486	1	0.3486	1.03	0.3347	
BC	0.6105	1	0.6105	1.80	0.2095	
A^2	4.81	1	4.81	14.16	0.0037	
B^2	6.02	1	6.02	17.74	0.0018	
C^2	2.98	1	2.98	8.77	0.0143	
Residual	3.39	10	0.3394			
Lack of fit	0.5281	5	0.1056	0.1843	0.9565	not significant
Pure error	2.87	5	0.5732			
Cor total	96.28	19				

this study was 30.40 with a *p*-value of 0.0001. This result proved that the model generated was statistically significant with only a 0.1% chance of noise occurrence. The variables of A, C, A^2, B^2, and C^2 had significant effects on the crystallinity since the *p*-values were less than 0.05. However, other variables were indicated as insignificant due to being higher than 0.05 of *p*-value. For single variables, variable B was identified as a limiting factor toward the optimization of HAp crystallinity. Since there was no influence of model reduction in insignificant variables, those insignificant variables were retained. The *F*-value with 'lack of fit' obtained was 0.1843 and the *p*-value was 0.9565 which implied that the lack of fit was not significantly relative to the pure error. Therefore, the relationship between crystallinity and the model was well within the chosen range.

This study also observed that the crystallinity, the pH, and the stirring rate were significant. These factors affected the crystallinity since the *p*-value was <0.05, implying the good factors. In acidic conditions, the phosphate ion, P, and Ca ion cannot combine to form the HAp crystal. However, HAp itself can self-integrate very well in alkaline conditions and forms a chemical bond between P and Ca (Goh *et al.* 2021). The maximum reaction of HAp produced in an alkaline condition compared to the acidic condition showed that the crystallinity is dependent on the pH of HAp.

For the stirring rate, the agglomeration between the particles will form a crystal and the speed of the stirring rate influences the size of crystallite and crystallinity since the particle agglomeration during the precipitation and maturation step controls the sizes of aggregates (Tourbin *et al.* 2020). Most particles are small and in micron size, and will become a greater proportion of larger agglomerates. As the stirring rates increase, the particle has a narrow size distribution, with most of the particles on a volume basic and having size between 1 and 10 μm (Baig *et al.* 2020; Molenaar *et al.* 2021). The fit statistic obtained from RSM showed the coefficient of determination R^2 was 0.9647, implying that 96.47% of the variability in the response can be explained by the quadratic model. Also, ought to be close to the value of 1 and considered significantly very high indicating that this model is highly reliable.

The difference between the predicted R^2 and the adjusted R^2 should be less than 0.2. In this study, the adjusted R^2 was 0.9330 and the predicted R^2 was 0.9094, the difference between these two values was only 0.02 which was less than 0.2 and, therefore, is an acceptable agreement. Adequate precision is a measurement of the experimental design signal-to-noise ratio which compares the range of predicted values at design points to average prediction error and a ratio that is >4 is desirable. Statistically, the value of adequate precision in this case was 19.3134, indicating an adequate signal that can be used to navigate the design space.

The best-fitting model was established by a regression analysis equation for the quadratic regression model formed according to the variable parameters (Halis & Kocakulak 2024). Fitting the data into various models and their subsequent ANOVA showed that crystallinity toward the production of HAp was suitably described with a quadratic polynomial model as in

Equation (3), in which the crystallinity units are in %, A is the pH, B is the contact time, and C is the stirring rate:

$$\text{Crystallinity} = 68.83 + 0.5181\ A + 0.2852\ B - 0.1063\ AB - 0.4303\ A^2 - 0.6608\ B^2 \quad (3)$$

Evaluation of the selected models consists of residual analysis. Residual can be defined as the difference between the experimental and predicted values by the model (Sun *et al.* 2022). Figure 2 shows a normal probability indicating the close residuals (Figure 1). These figures show that the data are well correlated.

The normal probability plot was closely accumulated at a certain point. These indicated an accurate model along with good agreement throughout the operating variables range as the residuals were distributed in a linear line (Regti *et al.* 2017). The normal distribution between the experimental and predicted values (Figure 1) indicated that the predicted result and the experimental result are highly similar and correlated strongly with each other. Although there were some points that showed slight deviation, most of the points were scattered in straight lines proving that there was great correspondence between the actual and predicted values (Bayuo *et al.* 2022). These plots (Figure 2(a) and 2(b)) were considered a good fit for the quadratic models.

Optimization of operating parameters was carried out to determine the best condition for the synthesis of HAp. Along with all parameters involved, the attempt to optimize the process parameter for HAp, for example optimum condition with optimum crystallinity and better purity. The optimum condition can be obtained by the response surface representing the contour plots with certain minimum and maximum response values obtained (Kavitha *et al.* 2015). The red dot on the top of the curve graph (Figure 3) represents the optimum condition for HAp production. The best condition was retrieved at a pH of 10, contact time of 48 h, and stirring rate of 180 rpm.

3.2. Identification of the type of HAp compounds produced

Table 2 presents the identification of compounds produced by RSM and was evaluated by the XRD analysis using PDXL software to match the spectra of the Joint Committee on Powder Diffraction Standard, JCPDS. From the XRD pattern search analysis, six of 20 experiment runs showed the formation of significant chemical structure of HAp compounds, indicating the suitable condition for phosphorus recovery from freshwater AQW. About four runs produced carbonated hydroxyapatite which indicated that the lower pH (below 10) is not enough for Ca^{2+} and PO_4^{3-} crystallization process.

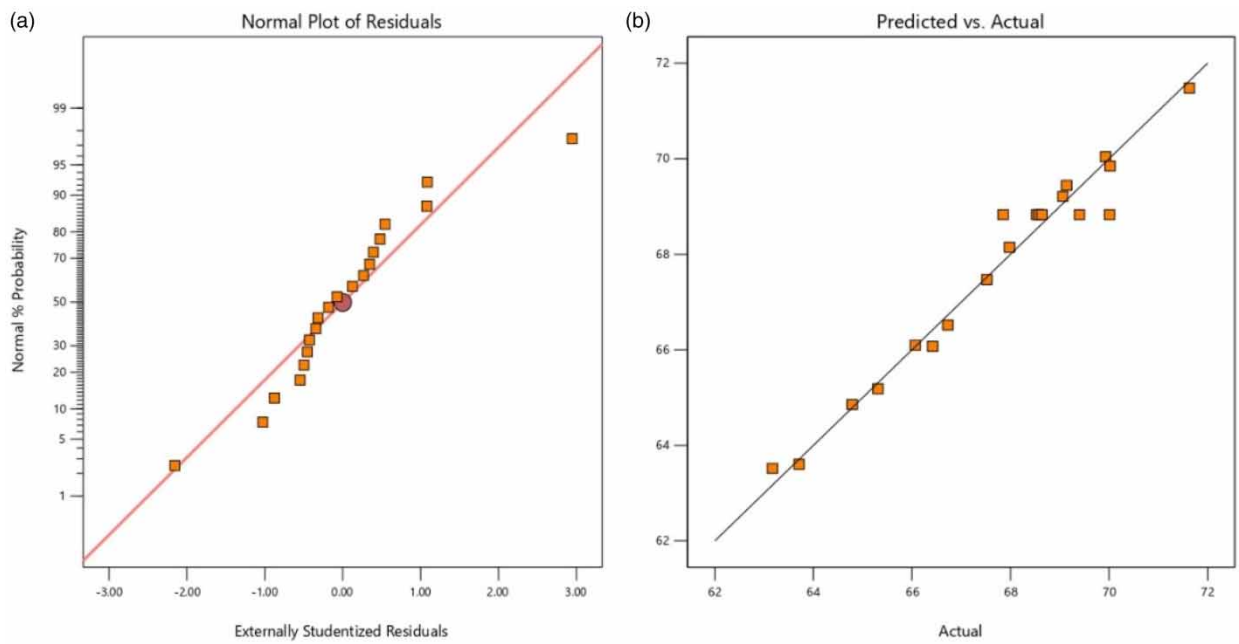

Figure 2 | Normal plot of residual graph (a) and the predicted vs. actual value graph (b).

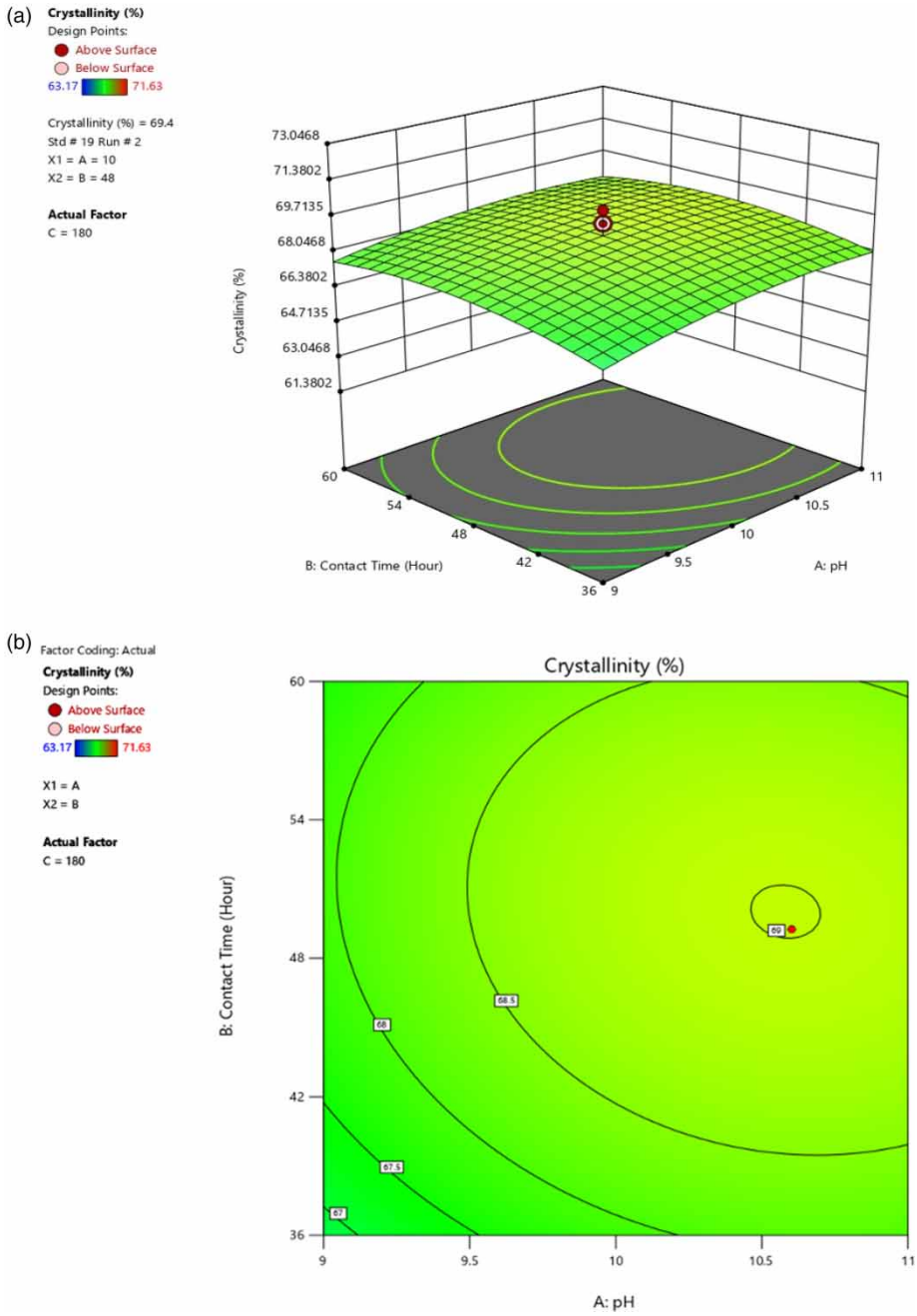

Figure 3 | The contour plot (a) in three-dimensional version and (b) in two-dimensional version, represent between the parameters and response.

According to Figure 4, HAp obtained from phosphate recovery (synthesis – Run 2) that was generated by RSM showed a different pattern compared to commercial HAp but the major peaks of HAp still appeared. Based on JCPDS 00-001-1008 (Joint Committee on Powder Diffraction Standard), the main intensity peaks of HAp appeared at level 20 and 2θ at 20–60°.

In addition, the CCD of the synthesized HAp exhibited a low-intensity peak which was considered low crystallinity since the calcination temperature was only at 100 °C but was still amorphous. However, low crystalline HAp exhibited a high biodegradation rate and was more metabolically active compared to high crystalline HAp (Alparslan 2017). The HAp CCD crystallite size was calculated using the Scherrer equation and the size obtained was 23.6 nm (Mohd Pu'ad *et al.* 2019).

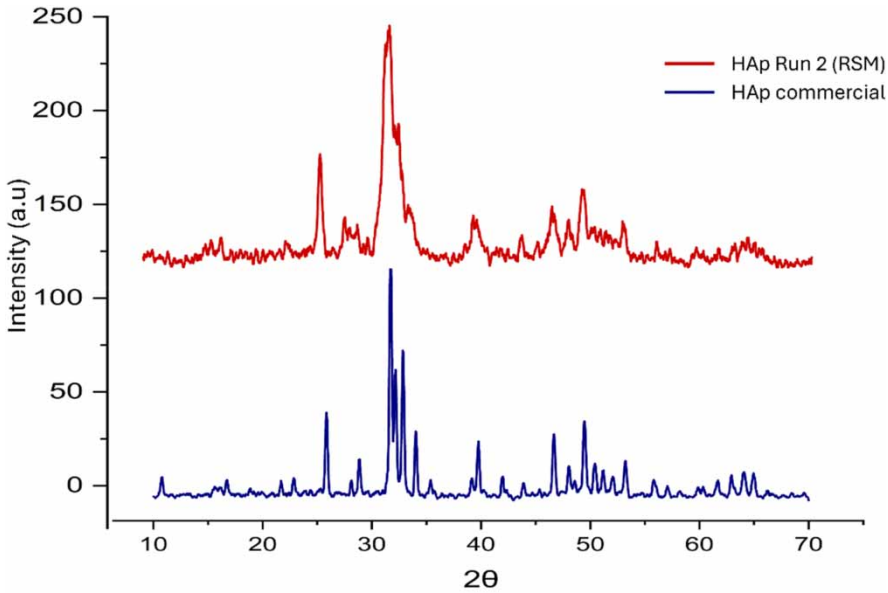

Figure 4 | XRD graph between synthesized HAp selected by CCD analysis and commercial HAp.

FTIR spectroscopy was used to determine the functional group of the selected compounds by RSM analysis; and the HAp compound is shown in Figure 5. The FTIR result showed that the bands at 551.64 and 606.37 cm^{-1} are attributed to the bending vibration phosphate (PO_4^{3-}) and at this region become doublet peak. This splitting bending mode vibration of PO_4^{3-} showed the transformation of HAp from amorphous to crystalline phase and this can be an index of crystallinity (Sroka-Bartnicka *et al.* 2017). The band at 1,020.75 cm^{-1} is the stretching vibration mode of PO_4^{3-}. The peaks present at 1,403.86 and 1,466.41 cm^{-1} are attributed to the carbonate group (CO^{2-}).

The peak at 3,311.58 cm^{-1} was assigned to the stretching mode of the hydroxyl group (OH^-). The band is relatively sideways from the broad peak for the O–H stretch vibration of hydrogen-bonded OH group (Poralan *et al.* 2015).

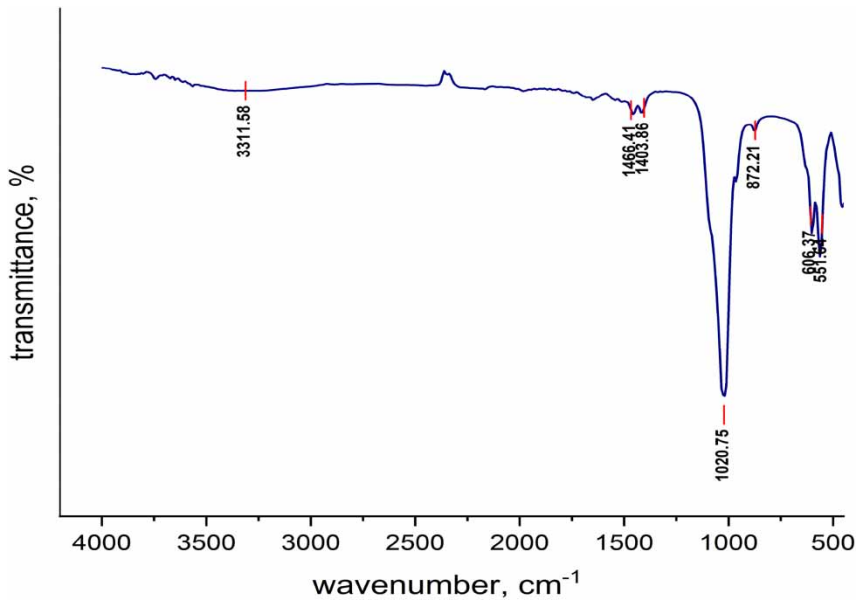

Figure 5 | FTIR graph of the synthesized HAp.

3.3. Recovery of phosphate ion in AQW

The AQW originally contained phosphorus concentrations between 17 and 23 ppm, which were added to achieve an optimal Ca/P ratio of 1.67 to produce HAp. After the synthesis of HAp, the phosphate concentration was measured and an impressive removal rate of 89.97% was observed, indicating successful optimization using RSM and CCD. Despite this success, a major challenge remains in optimizing the HAp production process for practical applications in wastewater treatment. Factors such as cost and availability of materials, and variations in wastewater composition are obstacles to large-scale implementation. To overcome these limitations, further research is required to assess scalability, cost efficiency, and operational robustness to ensure the feasibility and sustainability of the technology for practical use.

4. CONCLUSIONS

The goal for the present study, i.e. the optimization and characterization of HAp via RSM, was successfully achieved. This finding also proved that freshwater AQW can be recycled, with phosphorus being the most significant element that can be recovered. By chemical treatment with calcium as an adsorbent for phosphorus, the phosphate content in wastewater can be effectively reduced and converted into a valuable form. By running 12 experiment sets, the optimized conditions to produce HAp selected by RSM analysis were as follows: pH of 10, 48 h, and stirring rate of 180 rpm through a wet precipitate method. Statistically, RSM through CCD for optimization HAp showed that the quadratic model is significant. The FTIR result showed all the functional groups consisted of HAp while XRD showed the intensity and peaks of the commercial Hap, proving that this study was able to get almost similar HAp to the standard HAp. At the same time, this study managed to recover the uptake phosphate, and the phosphate recovery was around 89.97% which is considered as a good performance. For future research, the method could be extended to a larger industrial scale. Investigating alternative methods of phosphate recovery from wastewater and conducting thorough long-term environmental impact assessments are essential next steps. These assessments will be critical to making informed decisions and developing policies for the widespread implementation of such wastewater treatment and resource recovery methods.

ACKNOWLEDGEMENTS

The authors thank Universiti Malaysia Terengganu and the Ministry of Higher Education (MOHE) for providing the laboratory facilities and financial support, respectively. This work was supported by the Fundamental Research Grant Scheme (FRGS) (FRGS/1/2020/TK0/UMT/01/1).

DATA AVAILABILITY STATEMENT

All relevant data are included in the paper or its Supplementary Information.

CONFLICT OF INTEREST

The authors declare there is no conflict.

REFERENCES

Akpan, E. S., Dauda, M., Kuburi, L. S. & Obada, D. O. (2021) Box-Behnken experimental design for the process optimization of catfish bones derived hydroxyapatite: A pedagogical approach, *Materials Chemistry and Physics*, **272**, 124916.

Alparslan, Y. (2017) Extraction, characterization and antimicrobial activity of hydroxyapatite from seabass and seabream scale, *Journal of Food and Health Science* 3 (3), 92–93.

Anawar, H. M. & Chowdhury, R. (2020) Remediation of polluted riverwater by biological, chemical, ecological and engineering processes, *Sustainability (Switzerland)*, **12** (17), 2–3.

Baig, M., Cook, R., Pratten, J. & Wood, R. (2020) The effect of shape and size distribution of abrasive particles on the volume loss of enamel using micro-abrasion. *Wear* **448–449** (8), 203212.

Bayuo, J., Rwiza, M. & Mtei, K. (2022) Response surface optimization and modeling in heavy metal removal from wastewater – a critical review, *Environmental Monitoring and Assessment*, **194** (351). https://doi.org/10.1007/s10661-022-09994-7.

Chelladurai, S. J. S., Murugan, K., Ray, A. P., Upadhyaya, M., Narasimharaj, V. & Gnanasekaran, S. (2020) Optimization of process parameters using response surface methodology: A review. In *Materials Today: Proceedings*.

Cichy, B., Kużdżał, E. & Krztoń, H. (2019) Phosphorus recovery from acidic wastewater by hydroxyapatite precipitation, *Journal of Environmental Management*, **232**, 421–427.

Dadi, T., Schultze, M., Kong, X., Seewald, M., Rinke, K. & Friese, K. (2023) Sudden eutrophication of an aluminum sulphate treated lake due to abrupt increase of internal phosphorus loading after three decades of mesotrophy, *Water Research*, **235**, 119824.

Deng, W., Li, K. & Zhao, H. (2023) A flight arrival time prediction method based on cluster clustering-based modular with deep neural network, *IEEE Transactions on Intelligent Transportation Systems* PP (99), 1–10. DOI:10.1109/TITS.2023.3338251.

Deng, W., Cai, X., Wu, D., Song, Y., Chen, H., Ran, X., Zhou, X. & Zhao, H. (2024) MOQEA/d: Multi-objective QEA with decomposition mechanism and excellent global search and Its application, *IEEE Transactions on Intelligent Transportation Systems* **25** (6), 6238–6247.

Ebrahimi, A., Hajian, M. & Lotfi, I. (2014) Comparison study of turbidity removal using synthetized poly-aluminum chloride-sulfate and poly-aluminum chloride in aqueous solutions, *International Journal of Environmental Health Engineering*, **3** (1), 1–6.

Goh, K. W., Wong, Y. H., Ramesh, S., Chandran, H., Krishnasamy, S., Sidhu, A. & Teng, W. D. (2021) Effect of pH on the properties of eggshell-derived hydroxyapatite bioceramic synthesized by wet chemical method assisted by microwave irradiation, *Ceramics International*, **47** (7), 8879–8887.

Halis, S. & Kocakulak, T. (2024) RSM based optimization of lambda and mixed fuel concentration parameters of a LTC mode engine, *Energy*, **306**, 132550.

Jin, X., Rong, N., Zhang, W., Meng, X. & Shan, B. (2019) Bioavailability of organic phosphorus in an eutrophic lake: Insights from an in-situ experiment, *Ecological Indicators*, **107**, 105622.

Kavitha, M., Subramanian, R., Vinoth, K. S., Narayanan, R., Venkatesh, G. & Esakkiraja, N. (2015) Optimization of process parameters for solution combustion synthesis of Strontium substituted Hydroxyapatite nanocrystals using Design of Experiments approach, *Powder Technology*, **271**, 167–181.

Kurniawan, S. B., Abdullah, S. R. S., Imron, M. F., Ahmad, A., Mohd Said, N. S., Mohd Rahim, N. F., Mohammad Alnawajha, M., Abu Hasan, H., Othman, A. R. & Purwanti, I. F. (2021) Potential of valuable materials recovery from aquaculture wastewater: An introduction to resource reclamation, *Aquaculture Research*, **52** (7). https://doi.org/10.1111/are.15180.

Li, X., Xu, Y., Shen, S., Guo, T., Dai, H. & Lu, X. (2022) Effects of dissolved organic matter on phosphorus recovery via hydroxyapatite crystallization: New insights based on induction time, *Science of the Total Environment*, **822** (6). DOI:10.1016/j.scitotenv.2022.153618.

Li, X., Zhao, H. & Deng, W. (2024) IOFL: Intelligent optimization-based federated learning for non-IID data, *IEEE Internet of Things Journal*. PP (99), 1–1. DOI:10.1109/JIOT.2024.3354942.

Mat Zain, N. S. & Lee, L. K. (2022) Health complaints, mental status and quality of life among the aquaculture workers: A cross-sectional study in northern region of peninsular Malaysia, *International Journal of Environmental Research and Public Health*, **19** (23), 16371.

Mohd Pu'ad, N. A. S., Abdul Haq, R. H., Mohd Noh, H., Abdullah, H. Z., Idris, M. I. & Lee, T. C. (2019) Nano-size hydroxyapatite extracted from tilapia scale using alkaline heat treatment method. In *Materials Today: Proceedings*.

Molenaar, R., Chatterjee, S., Kamphuis, B., Segers-Nolten, I. M. J., Claessens, M. M. A. E. & Blum, C. (2021) Nanoplastic sizes and numbers: Quantification by single particle tracking, *Environmental Science: Nano*, **8** (3). DOI:10.1039/D0EN00951B.

Nizam, N. U. M., Hanafiah, M. M., Noor, I. M. & Karim, H. I. A. (2020) Efficiency of five selected aquatic plants in phytoremediation of aquaculture wastewater, *Applied Sciences (Switzerland)*, **10** (2712), 1–11.

Poralan, G. M., Gambe, J. E., Alcantara, E. M. & Vequizo, R. M. (2015) X-ray diffraction and infrared spectroscopy analyses on the crystallinity of engineered biological hydroxyapatite for medical application. In: *IOP Conference Series: Materials Science and Engineering*.

Regti, A., Laamari, M. R., Stiriba, S. E. & El Haddad, M. (2017) Use of response factorial design for process optimization of basic dye adsorption onto activated carbon derived from Persea species, *Microchemical Journal*, **130**, 129–136.

Sadat-Shojai, M., Khorasani, M. T., Dinpanah-Khoshdargi, E. & Jamshidi, A. (2013) Synthesis methods for nanosized hydroxyapatite with diverse structures, *Acta Biomaterialia*, **9** (8), 7591–7621.

Sajid, M. & Płotka-Wasylka, J. (2020) Nanoparticles: Synthesis, characteristics, and applications in analytical and other sciences, *Microchemical Journal*, **154**, 104623.

Schindler, D. W., Carpenter, S. R., Chapra, S. C., Hecky, R. E. & Orihel, D. M. (2016) Reducing phosphorus to curb lake eutrophication is a success, *Environmental Science and Technology*, **50** (17). doi/10.1021/acs.est.6b02204.

Shrestha, S., Wang, B. & Dutta, P. (2020) Nanoparticle processing: Understanding and controlling aggregation, *Advances in Colloid and Interface Science*, **279**, 102162.

Singh, A. K. (2021) An inclusive study on new conceptual designs of passive solar desalting systems, *Heliyon*, **7** (2), e05793. http://www.cell.com/article/S2405844020326360/fulltext (Accessed April 1, 2024).

Singh, A. K. (2023) Mathematical analysis of optimized requisites for novel combination of solar distillers, *Journal of Engineering Research*, **11** (4), 515–525.

Singh, A. K. & Samsher (2021) Material conscious energy matrix and enviro-economic analysis of passive ETC solar still, *Materials Today: Proceedings*, **38**, 1–5.

Singh, A. K. & Samsher (2022) Tech-en-econ-energy-exergy-matrix (T4EM) observations of evacuated solar tube collector augmented solar desaltification unit: A modified design loom, *Materials Today: Proceedings*, **61**, 258–263.

Sroka-Bartnicka, A., Borkowski, L., Ginalska, G., Ślósarczyk, A. & Kazarian, S. G. (2017) Structural transformation of synthetic hydroxyapatite under simulated in vivo conditions studied with ATR-FTIR spectroscopic imaging, *Spectrochimica Acta – Part A: Molecular and Biomolecular Spectroscopy*, **171**, 155–161.

Sun, X., Abbass, R., Ghoroqi, M., Patra, I., Dwijendra, N. K. A., Uktamov, K. F. & Jasem, H. (2022) Optimization of dyes and toxic metals removal from environmental water samples by clinoptilolite zeolite using response surface methodology approach, *Scientific Reports*, **12** (1). DOI:10.1038/s41598-022-17636-8.

Tiwari, A. K. & Pal, D. B. (2022) Nutrients contamination and eutrophication in the river ecosystem. In: *Ecological Significance of River Ecosystems: Challenges and Management Strategies* (Madhav, S., Kanhaiya, S., Srivastav, A. L., Singh, V. B. & Singh, P., eds.). Elsevier, Amsterdam, pp. 203–216.

Tourbin, M., Brouillet, F., Galey, B., Rouquet, N., Gras, P., Abi Chebel, N., Grossin, D. & Frances, C. (2020) Agglomeration of stoichiometric hydroxyapatite: Impact on particle size distribution and purity in the precipitation and maturation steps, *Powder Technology*, **360**. 981–983.

Yang, C., Li, J. & Yin, H. (2022) Phosphorus internal loading and sediment diagenesis in a large eutrophic lake (Lake Chaohu, China), *Environmental Pollution*, **292**, 2–3.

First received 9 December 2023; accepted in revised form 10 August 2024. Available online 21 August 2024